

Nonequilibrium dynamics induced by scattering forces for optically trapped nanoparticles in strongly inertial regimes

Yacine Amarouchene^{1,*}, Matthieu Mangeat¹, Benjamin Vidal Montes¹,

Lukas Ondic², Thomas Guérin¹, David S. Dean¹, and Yann Louyer^{1†}

(1) *Univ. Bordeaux, CNRS, LOMA, UMR 5798, F-33400 Talence, France and*

(2) *Institute of Physics, Academy of Sciences of the Czech Republic, CZ-162 00 Prague, Czech Republic.*

(Dated: September 4, 2022)

As a first approximation, the forces acting on optically trapped particles are commonly assumed to be conservative. The influence of the nonconservative force has been shown to be negligible in overdamped liquid environments. However, its impact in the underdamped regime remains unexplored. Here, we experimentally study the combined effects of gradient and scattering forces on the nonlinear dynamics of trapped particles at various air pressures, leading to significant low-frequency noise excess along the optical axis and the emergence of toroidal Brownian vortices. Our results supported, by numerical simulations and a theoretical model, provide fundamental insights into the functioning of optical tweezers and a means for investigating nonequilibrium steady states in the presence of nonconservative forces.

The pioneering works of Arthur Ashkin, in the 1970s through to the mid-1980s, on the optical control and manipulation of dielectric particles have led to major advances in cold atom physics and biophysics. By tightly focusing a laser beam, Ashkin showed how to trap a particle in liquid environment using the intensity gradient force of a laser [1]. Notably, it is only recently that the gradient force has been used to trap dielectric particles in vacuum [2, 3], leading to impressive proposals and experimental results in ultra-weak force sensing and fundamental tests of quantum mechanics [4–11]. In most of the applications, the optical potential of a single-beam trap can be considered as harmonic. Anharmonicities are known to be important at sufficiently low friction, where the particle can explore them [14]. In these studies, the particle’s motion is described via a Duffing oscillator, whose nonlinear components arise solely from the gradient force [14–16]. However, another source of anharmonicity is related to scattering forces with nonconservative components. Nonconservative forces are known to induce steady-state non-equilibrium probability currents, which are made manifest by so called Brownian vortices, these have been demonstrated both theoretically and experimentally for trapped overdamped Brownian particles [17, 18]. The effect of such forces is modest in the overdamped regime [20, 21]. However, experimental and theoretical studies on scattering forces acting on the particle in the strongly inertial regime (underdamped regime), have not yet been reported and may play a crucial role for the particle loss at low pressure [10].

In this Letter, we study the influence of scattering forces, in the nonlinear regime, on optically trapped nanoparticles in near vacuum. We observe, for the first time in an optical trap, pressure-dependent additional low-frequency broadband axial positional fluctuations, which we explain theoretically. Such effects dominate over thermal fluctuations for this frequency range. These low-frequency contributions in the axial motion originate from the scattering forces and are further amplified by

the nonlinear gradient components. In the context of a Duffing potential tilted by an additive homogeneous force, a low-frequency mode has already been observed in analog circuits without nonconservative forces [22]. Our results show that nonconservative forces are necessary to describe the complete dynamics of the trapped particle, including the emergence of Brownian vortices. This Letter is accompanied by a theoretical article [23], which provides complements and insights in to the functioning of optical trapping, while proposing extensions of our experimental work for future studies.

Similarly to Ref. [3], we construct, inside a vacuum chamber, a linearly polarized single-beam gradient trap by focusing a low-noise $\lambda = 1064$ nm laser (430 mW power) with a high 0.8 numerical aperture objective. Nebulization of a dilute solution of fused silica nanoparticles (density, $\rho = 2200$ kg.m⁻³, refractive index $n = 1.45$, with a nominal diameter of 136 nm and a standard deviation of 5 nm) in ethanol leads to the trapping of a single particle at ambient pressure for days. The particle’s trajectory in 3D is measured by forward scattered light interferometry [2] and recorded with a sample rate of 10 MS/s (16 bits of vertical resolution) with more than 3×10^6 points for each axis. We compute power spectral densities (PSDs) from time traces of the particle’s motion along the three axes (with a typical noise floor \sim pm²/Hz). For clarity, we only present results for the x transverse and z axial components. Fig. 1(a) displays PSDs for several pressures. Upon lowering the pressure, the system crosses from the quasi-linear to the non-linear regime [14]. We observe a clear transition towards non-symmetric lineshapes below roughly 1 mbar induced by nonlinearities.

It is necessary to, first, quantify the three-dimensional stochastic Duffing oscillator both for calibration purposes but also to infer the beam parameters w_j ’s used later for analyzing the role of the radiation pressure and to determine the center of mass motion temperature. For weak displacements $x_i = x, y$ or z of the particle, relative to the

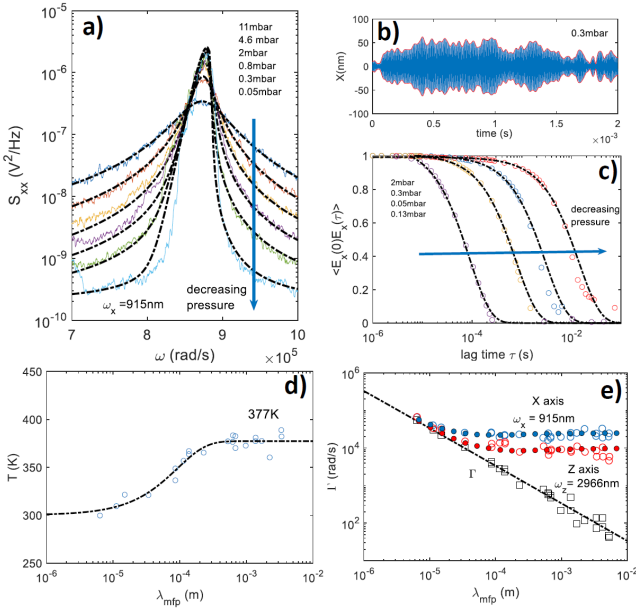


FIG. 1. a) Power Spectral Densities PSDs S_{xx} along the transverse x axis for several pressures. The dashed lines correspond to fits to the data using the theoretical expression Eq. (2). b) Typical time trace along the x axis. c) Normalized Energy correlation functions with exponential fits. d) Center of mass motion temperature T versus mean free path λ_{mfp} . e) Effective damping rates measured either by looking at the FWHM of the PSD along x (blue circles) and z axis (red circles) or the inverse of the correlation time in c) (black squares). The dashed line is a fit to the data using Eq. (1) with a single fitting parameter $R_p = 68\text{nm}$. The blue and red closed symbols correspond to the FWHM of the PSD of the theoretical model [see Eq. (2)].

trapping laser wavelength λ , we calculate to first order in the x_i the optical forces assuming the Gaussian Beam approximation [14]. A softening of the effective stiffness $\kappa_i^{\text{eff}}(\mathbf{x}) = \kappa_i \left(1 - \sum_{j=x,y,z} \xi_{ij} x_j^2\right)$, *i.e.* due to nonlinearities, in the gradient force $F_i^{\text{grad}} = -\kappa_i^{\text{eff}}(\mathbf{x})x_i$ is experimentally observed through the frequency shift of the linear resonance $\Omega_i = (\kappa_i/m)^{1/2}$, leading to asymmetric profiles in the PSDs rather than the usual Lorentzian arising in the linear regime [14]. Here κ_i is the linear trap stiffness, seen by the coordinate x_i , and m the mass of the particle. Duffing nonlinearities are quantified by the coefficients $\xi_{ij} = 2/w_j^2$ except for $\xi_{zj=x,y} = 4/w_j^2$, where $w_{j=x,y}$ are the beam waist radii and $w_{j=z}$ is the Rayleigh length. The theory of a 1D underdamped anharmonic oscillator undergoing random thermal motion has been already described in [16, 24]. To calculate spectral densities [24], we adapt this theory to the 3D case (with the secular approach [14, 15]). The theoretical analysis is based on two parameters, the damping rate Γ and an anharmonicity parameter α_i^R quantifying the strength of nonlinearities $\alpha_i^R = \frac{3}{4}C_i\xi_{ii}k_B T/m\Omega_i\Gamma$ with $C_{i=x,y} = 9/4$, $C_{i=z} = 7/2$ [15] and where k_B is the Boltzmann constant.

This analysis is valid in the underdamped ($\Gamma \ll \Omega_i$) and low-temperature regimes ($\alpha_i^R\Gamma \ll \Omega_i$). Finally, the damping coefficient of the particle in a rarefied gas is taken to be [2, 25]

$$\Gamma = \frac{6\pi\eta R_p}{m} \frac{0.619}{0.619 + Kn} (1 + c_K), \quad (1)$$

where R_p is the particle's radius and η the viscosity of air. The dependence of Γ with the gas pressure P depends on the Knudsen number $Kn = \lambda_{\text{mfp}}/R_p$, where $\lambda_{\text{mfp}} = \lambda_{\text{mfp}0} \cdot P_{\text{atm}}/P$ is the mean free path of air molecules with P_{atm} and $\lambda_{\text{mfp}0} = 68\text{nm}$ being respectively the atmospheric pressure at 20°C and the corresponding mean free path. The additional correction in Kn is given by $c_K = (0.31Kn)/(0.785 + 1.152Kn + Kn^2)$. In the limit $Kn \gg 1$, we find $\Gamma \propto P$. In terms of the hypergeometric function ${}_2F_1$, the spectral density of the fluctuations of the coordinate x_i is then given by [24]

$$S_{ii}(\omega) = \frac{k_B T}{m\Omega_i^2} \sum_{l=\pm 1} \text{Re} \left\{ \frac{(1+q_i)^{-4} \frac{16q_i}{\Gamma(\kappa_i^i(\omega)+1)} \times}{{}_2F_1(2, \kappa_i^i(\omega)+1, \kappa_i^i(\omega)+2; \xi_i)} \right\}, \quad (2)$$

with $q_i = (1 + 4i\alpha_i^R)^{1/2}$, $\kappa_i^i(\omega) = -(\Gamma/2 - i[l\omega + \Omega_i - \Gamma^2/8\Omega_i])/q_i\Gamma$, and $\xi_i = -(1/4\alpha_i^R)^2(1 - q_i)^4$. We calibrate the optical tweezer at relatively high pressures ($T = 300\text{K}$), that is, in the weakly nonlinear regime ($\alpha_i^R \ll 1$) where the spectral density is given by

$$S_{ii}(\omega) = \frac{2k_B T}{m} \frac{\Gamma_i^e}{([\Omega_i^e]^2 - \omega^2)^2 + (\omega\Gamma_i^e)^2}. \quad (3)$$

Eq. (3) corresponds to a single Lorentzian line with renormalized resonance frequency $\Omega_i^e = \Omega_i + 2\alpha_i^R\Gamma - \Gamma^2/8\Omega_i$ and the linewidth $\Gamma_i^e = \Gamma \left(1 + 4[\alpha_i^R]^2\right)$.

We now present a new nonlinear calibration method performed as follows:

1) We fit the PSDs at high pressure with the Lorentzian form given in Eq. (3), where they are indeed well approximated by a Lorentzian form, to determine the effective eigenfrequencies Ω_i^e and damping Γ_i^e . Using the nominal nanoparticle size given by the manufacturer to estimate Γ via Eq. (1) then provides a first estimate for α_i^R .

2) The extraction of both the local envelope amplitude $\langle x^2(t) \rangle^{1/2}$ and the local frequency $\Omega_x(t)$ allows for a measurement of the time resolved energy potential energy associated with the direction x , $E_x(t) = m\Omega_x^2(t)x^2(t)/2$. Its correlation function decreases exponentially as expected with a characteristic time Γ^{-1} as shown in Fig. 1(c) [16]. The size of the particle is then verified independently using Eq. (1). We find a particle radius $R_p = 68\text{nm}$ (*i.e.* the nominal size given by the manufacturer).

3) Fitting Lorentzian PSDs with effective eigenfrequencies Ω_i^e and damping Γ_i^e at high pressure allows the

calibration from volts V to meters for each axis. This is via the determination of the prefactor $2k_B T/m$ in Eq. (3) where (i) we take $T = 300K$ in the high pressure data as the gas density is assumed sufficient to equilibrate the particle temperature with that of the surrounding gas (ii) m is determined from R_p and the density of SiO_2 given earlier. We then use Eqs. (2) to fit the spectral densities [Fig. 1(a)] between the regimes of weak and strong nonlinearities, where the slight discrepancy seen in the wings of PSDs are due to a lack of statistics at low pressure and to the 10^{-3} relative laser power fluctuations. This step is performed iteratively to minimize the error between the experimental FWHM (Full Half Width Maximum) of PSDs and FWHM given by the nonlinear theory Eqs. (2).

4) The temperature T of the system in the low pressure regime is deduced relative to the ambient temperature (*i.e.* 300 K as reference at high pressure for $\alpha_i^R < 1$), for which the calibration has been carried out using Eqs. (3-2) as shown in Fig. 1(d).

The final trap parameters obtained from this procedure are: $w_x = 0.915 \mu\text{m}$, $w_y = 1.034 \mu\text{m}$ and $w_z = 2.966 \mu\text{m}$. Fig. 1(e) clearly shows a saturation of the linewidths Γ_i^e , that is well reproduced by the full height maximum widths FHMW given by Eq. (2). As soon as $\alpha_i^R > 1$, the widths deviate from each other such that $\Gamma_x^e > \Gamma_z^e$, meaning that $\alpha_x^R > \alpha_z^R$. The knowledge of these geometrical parameters of the focused laser beam are crucial for the analysis of the influence of scattering forces, as we shall now demonstrate.

In what follows, we present evidence of the influence of the scattering force on the dynamics of the particle. We numerically solve the 3D nonlinear Langevin equations for distinct situations and calculate the respective PSDs [26]. For $|x_i| \ll \lambda$, the longitudinal nonconservative force is given by $F_z^{\text{scatt}} = \frac{\alpha''}{\alpha'} \kappa_z \left(\gamma_0 + \sum_{i=x,y,z} \gamma_i x_i^2 \right)$, where α' and α'' are, respectively, the real and imaginary parts of the effective polarizability $\alpha = \alpha_0 / [1 - ik^3 \alpha_0 / (6\pi\epsilon_0)]$, with $k = 2\pi/\lambda$ and ϵ_0 the vacuum permittivity [14]. Physically, the optical forces arise from the interaction between the electromagnetic field of the Gaussian beam and the polarizability $\alpha_0 = 4\pi\epsilon_0 R_p^3 (\epsilon - 1) / (\epsilon + 2)$ of a spherical object of dielectric constant ϵ . The coefficients γ depend on the geometrical parameters of the focused laser: $\gamma_0 = w_z(w_z k - 1)$, $\gamma_{i=x,y} = k/2 + 2(w_z - kw_z^2)/w_i^2$ and $\gamma_z = (2 - w_z k)/w_z$ [14].

Our numerical simulations reveal that the transverse scattering forces $F_{i=x,y}^{\text{scatt}}$ have a negligible contribution in the frequency and position fluctuations. In the first case, we let $F^{\text{scatt}} = 0$ (*Duffing case*) while in the two other situations the scattering force is taken into account with (*Fully nonlinear*) and without the Duffing terms (*scattering model*) at $P = 0.1$ mbar. In the latter case, Duffing terms and the homogeneous force $F_z^{\text{scatt}} = \frac{\alpha''}{\alpha'} \kappa_z \gamma_0$ are used for comparison with previous works [22]. This *tilted Duffing* model clearly overestimates the low-frequency re-

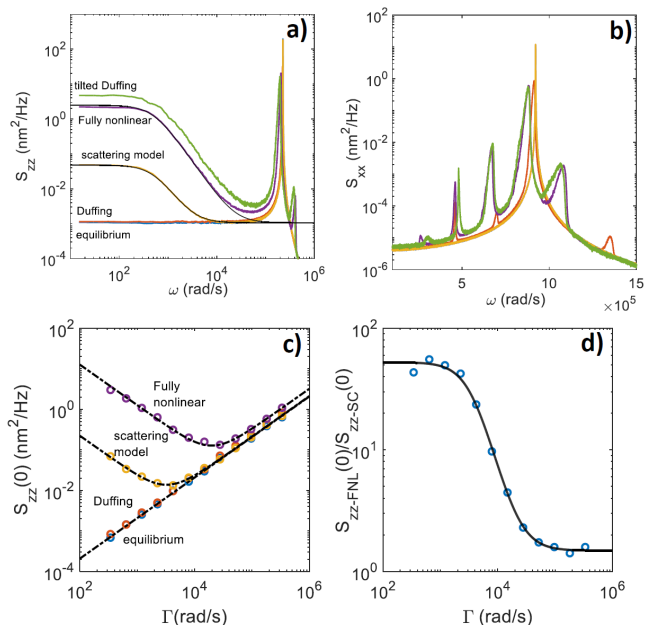


FIG. 2. Numerical simulation results using the waists w_i extracted from the nonlinear calibrations at a pressure of 0.1mbar. PSDs S_{ii} along $i = z$ axis (a) and $i = x$ axis (b) for the different cases described in the text. c) $S_{zz}(0)$ versus damping rate Γ . d) Ratio of the zero frequency response $S_{zz}(0)$ for the fully nonlinear case and the scattering model (see text).

sponse [Fig. 2(a)].

The *scattering model* that is presented in detail in the companion paper [23] allows us to understand the interplay of the thermal fluctuations with the scattering force in the weak damping and low temperature regime [16]. This simple analytical model disregards Duffing nonlinearities, axial z dependent nonlinear terms in F_z^{scatt} and assumes $F_{i=x,y}^{\text{scatt}} = 0$. Thus, the scattering force only appears in the evolution of the axial motion through $F_z^{\text{scatt}} = \epsilon \kappa a [1 - (x^2 + y^2)/a^2]$, with $\epsilon = \frac{\alpha''}{\alpha'} (\kappa_z/\kappa) \sqrt{\gamma_0 |\gamma_{xy}|}$ and $a = \sqrt{\gamma_0 / |\gamma_{xy}|}$ [20]. This simplified model is sufficient to describe the main aspects of the particle motion $z(t)$ and is consistent with numerical simulations. For clarity, we assume an isotropic transverse trap. Consequently, $\kappa(\gamma_{xy})$ are the mean values of $\kappa_x, \kappa_y(\gamma_x, \gamma_y)$. The axial low-frequency PSDs $S_{zz}(\omega)$ along z is given by [23]

$$S_{zz}(\omega) = \frac{2k_B T \Gamma}{m \Omega_z^4} + 4 \left(\frac{\epsilon k_B T}{a m \Omega_z^2} \right)^2 \frac{\Gamma}{\Gamma^2 + \omega^2}. \quad (4)$$

Fig. 2(a-b) show how F^{scatt} increases the frequency shift of the resonance by a few percent. More importantly, we see that F^{scatt} leads to broadband axial position fluctuations, which are further enhanced by the Duffing terms. Note that these low-frequency overdamped

fluctuations are absent in the transverse spectral densities (data not shown). The transverse dynamics is only affected around the resonance frequency for which nonlinear couplings are seen in Fig 2(b). Eq. (4) perfectly reproduces the numerical simulation of $S_{zz}(\omega)$ for the *scattering model* (see Fig.2(a) and [23]) and shows that the low-frequency overdamped component (only visible in the axial direction) has a corner frequency given by Γ . The Γ dependence of the amplitude $S_{zz}(0)$ for the different cases described above are shown in Fig. 2(c). Strikingly, the theory also gives good fitting results for the fully nonlinear regime at low frequency provided that a pressure dependent correction factor $S_{zz-FNL}(0)/S_{zz-SC}(0)$ (shown in Fig. 2d) is used solely for the scattering correction term in Eq. (4).

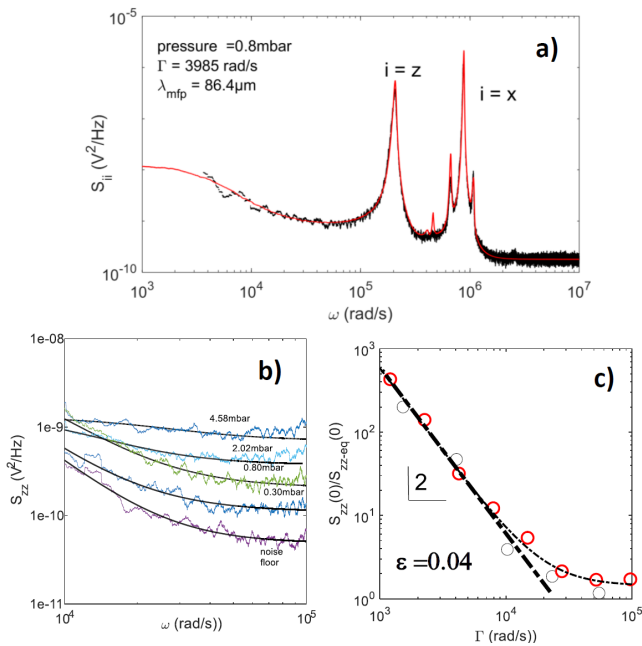


FIG. 3. a) Experimental PSDs (x and z) versus fully nonlinear simulation of the PDSs at a pressure of 0.8 mbar (black experiments/red simulations. (idem for c)). b) Low frequency part of $S_{zz}(\omega)$ at various pressures. The fits to the data correspond to a fit using Eq. (4). The deduced values of $S_{zz}(0)$ relative to the equilibrium value versus the damping rate Γ is shown in c). The thin line is a guide to the eye while the thick line highlights the Γ^2 scaling discussed in the text.

Experimentally, the low-frequency $1/f$ -like noise of the laser hinders the direct observation of $S_{zz}(0)$. To circumvent this technical issue, Fig. 3(a) displays the raw experimental PSDs $S_{ii}(\omega) = c_x S_{xx}(\omega) + c_z S_{zz}(\omega)$ for a limited range of frequencies at 0.8 mbar (c_x and c_z being calibration constants). These experimental data are in good agreement with our numerical simulations using the calibration factors and the beam parameters previously determined. Fig. 3(b) displays the pressure dependence of the low-frequency response of the PSDs along the z axis. Knowing Γ for each pressure, fitting of Eq. (4) enables us to infer $S_{zz}(0)$ relative to its equilibrium value

$S_{zz-eq}(0)$ as shown in Fig. 3(c). The expected scaling for $S_{zz}(0)/S_{zz-eq}(0) \sim 2 \frac{k_B T}{m} \left(\frac{\varepsilon}{a}\right)^2 \frac{1}{\Gamma^2}$ is observed at low pressures for the *scattering model*. Using corrections in temperature shown in Fig. 1(d) and due to nonlinearities in Fig. 2(d) provides a means to estimate $\varepsilon \approx 0.04$ corresponding to an imaginary index of $\approx 10^{-7}$, as expected for fused silica [27].

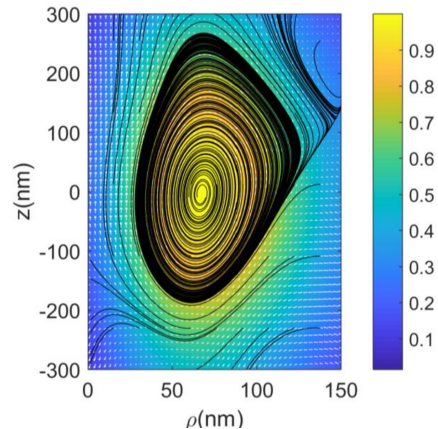


FIG. 4. Streamlines of the current density \mathbf{J} in the (ρ, z) plane for an experiment at a pressure $P = 10.8$ mbar. The color bar displays the steady probability distribution $P_s(\rho, z)$.

The effect of the scattering force in optical tweezers was first revealed by the presence of toroidal Brownian vortices or rolls (non-equilibrium currents) in liquid environments [17–19]. The question arises as to whether there are such currents when the particle is underdamped, intuitively this should be the case. From the complete experimental 3D trajectories, we computed the essential quantities [23] to detect these rolls, namely the steady state probability distribution $P_s(\mathbf{x})$ and the current density $\mathbf{J}_x(\mathbf{x}) = \langle \mathbf{V}(\mathbf{x}) \rangle P_s(\mathbf{x})$ in position space where $\langle \mathbf{V}(\mathbf{x}) \rangle$ is the corresponding mean velocity at the point $\mathbf{x} = (\rho, z)$. Both $P_s(\mathbf{x})$ and $J_x(\mathbf{x})$ are estimated either by a 6-dimensional histogram binning [19] or kernel density techniques [17]. Fig. 4 presents the experimental current density at a pressure of 10.8 mbar for a projection on the polar coordinate $\rho = (x^2 + y^2)^{1/2}$. A clear Brownian vortex is present in the (ρ, z) -plane, whose center lies close to the mean equilibrium position. This is qualitatively consistent with predictions made in the companion theoretical article [23], where nonconservative scattering forces on trapped Brownian particles in all damping regimes [23] are treated perturbatively (but in the absence of nonlinear Duffing terms) for $\varepsilon \ll 1$.

In summary, we have experimentally and theoretically demonstrated the effect of radiation pressure for optically trapped nanoparticles in the nonlinear underdamped regime. In a near vacuum environment, position fluctuations are amplified at low pressure. Toroidal Brownian vortices have also been observed, and these findings deserve future study. In particular, understand-

ing the exact topology of Brownian vortices (in position-velocity space) and their efficiencies versus dissipation require further experimental investigation in the underdamped regime [18, 28], but also paves the way towards studying the time reversal symmetry breaking induced by non conservative forces [23]. Our work opens a new pathway for study of nonequilibrium statistical physics for a wide range of damping regimes. It also highlights the importance of fully characterizing optical traps in the quest of ultra-weak force sensing and fundamental tests of quantum mechanics.

We thank L. Haelman for the construction of the vacuum chamber, W. Benharbone, S. Cassagnere and B. Tregon from the Electronics Lab, and R. Avriller for stimulating discussions. This work was partially funded by the Bordeaux IdEX program - LAPHIA (ANR-10-IDEX-03-02) -Arts et Science (Sonotact 2017-2018) and Projet Region Aquitaine (2018-1R50304).

* yacine.amarouchene@u-bordeaux.fr

† yann.louyer@u-bordeaux.fr

- [1] A. Ashkin, *Optical Trapping and Manipulation of Neutral Particles Using Lasers*, World Scientific Publishing (2006) and references therein.
- [2] T. Li, S. Kheifets, and M.G. Raizen, *Nature Physics* **7**, 527 (2011).
- [3] J. Gieseler, B. Deutsch, R. Quidant, and L. Novotny, *Phys. Rev. Lett.* **109**, 103603 (2012).
- [4] A. Arvanitaki and A. Geraci, *Phys. Rev. Lett.* **110**, 071105 (2013).
- [5] A. B. K. Lochan, S. Satin, T. Singh, and H. Ulbricht, *Rev. Mod. Phys.* **85**, 471 (2013).
- [6] J. Bateman, S. Nimmrichter, K. Hornberger, and H. Ulbricht, *Nat. Commun.* **5**, 4788 (2014).
- [7] D. Moore, A. Rider, and G. Gratta, *Phys. Rev. Lett.* **113**, 251801 (2014).
- [8] G. Ranjit, D. Atherton, J. Stutz, M. Cunningham, and A. Geraci, *Phys. Rev. A* **91**, 051805 (2016).
- [9] A. Rider, D. Moore, C. Blakemore, M. Louis, M. Lu, and G. Gratta, *Phys. Rev. Lett.* **117**, 101101 (2016).
- [10] G. Ranjit et al., *Phys. Rev. A* **91**, 051805 (2015); G. Ranjit et al., *Phys. Rev. A* **93**, 053801 (2016).
- [11] J. Liu and K.-D. Zhu, *Phys. Rev. D* **95**, 044014 (2017).
- [12] J. Millen, T. Deesuwana, P. Barker and J. Anders, *Nature Nanotechnology* **9**, 425 (2014).
- [13] J. Vovrosh, M. Rashid, D. Hempston, J. Bateman, and H. Ulbricht, *JOSAB* **34**, 1421 (2017).
- [14] J. Gieseler, L. Novotny and R. Quidant, *Nature Physics* **9**, 806 (2013).
- [15] M. Yoneda and K. Aikawa, *J. Phys. B: At. Mol. Phys.* **50**, 245501 (2017).
- [16] Dykman, M.I. and Krivoglaz, *Phys. Stat. Sol. B.* **48**, 497 (1971); Dykman and M.I., Krivoglaz, *M.A. Physica A: Statistical Mechanics and its Applications*, **104**, 495 (1980).
- [17] Y. Roichman, B. Sun, A. Stolarski, and D. Grier, *Phys. Rev. Lett.* **101**, 128301 (2008).
- [18] H. W. Moyses, R.O. Bauer, A.Y. Grosberg, and D. Grier, *Phys. Rev. E* **91** 062144 (2015).
- [19] P. Wu, R. Huang, C. Tischer, A. Jonas, and E.-L. Florin, *Phys. Rev. Lett.* **103** 108101 (2009).
- [20] M. de Messieres, N. A. Denesyuk, and A. La Porta, *Phys. Rev. E* **84** 031108 (2011).
- [21] G. Pesce, G. Volpe, A. C. De Luca, G. Rusciano, and G. Volpe, *EPL* **86**, 38002 (2009).
- [22] Dykman, M.I., Mannella, R., McClintock, P.V.E., Soskin, S.M., Stocks, N.G., *Physical Review A.* **43**, 1701 (1991); Dykman, M.I., Mannella, R., McClintock, P.V.E., Soskin, S.M., Stocks, N.G., *Physical Review A.* **42**, 7041 (1990).
- [23] M. Mangeat, Y. Amarouchene, Y. Louyer, T. Guérin, and D.S. Dean, submitted as the companion article.
- [24] W. Renz, *Z. Phys. B - Condensed Matter* **59**, 91 (1985).
- [25] S. A. Beresnev, V. G. Chernyak, and G. A. Fomyagin, *J. Fluid Mech.* **219**, 405 (1990).
- [26] D. A. Sivak, J. D. Chodera and G. E. Crook, *J. Phys. Chem. B*, **118**, 6466 (2014).
- [27] R. Kitamura, L. Pilon, and M. Jonasz, *Appl. Opt.* **46**, 8118 (2007).
- [28] D. Ruffner, and D. G. Grier, *Phys. Rev. Lett.* **108**, 173602 (2012).